Flexible Fault-Tolerant Topology for Switched Reluctance Motor Drives

Yihua Hu, *Senior Member, IEEE*, Chun Gan, *Student Member, IEEE*, Wenping Cao, *Senior Member, IEEE*, Jiangfeng Zhang, Wuhua Li, *Member, IEEE*, and Stephen J. Finney

***Abstract*—Switched reluctance motor (SRM) drives are one competitive technology for traction motor drives. This paper proposes a novel and flexible SRM fault-tolerant topology with fault diagnosis, fault tolerance, and advanced control functions. The converter is composed of a single-phase bridge and a relay network, based on the traditional asymmetrical half-bridge driving topology. When the SRM-driving system is subjected to fault conditions including open-circuit and short-circuit faults, the proposed converter starts its fault-diagnosis procedure to locate the fault. Based on the relay network, the faulty part can be bypassed by the single-phase bridge arm, while the single-phase bridge arm and the healthy part of the converter can form a fault-tolerant topology to sustain the driving operation. A fault-tolerant control strategy is developed to decrease the influence of the fault. Furthermore, the proposed fault-tolerant strategy can be applied to three-phase 12/8 SRM and four-phase 8/6 SRM. Simulation results in MATLAB/Simulink and experiments on a three-phase 12/8 SRM and a four-phase 8/6 SRM validate the effectiveness of the proposed strategy, which may have significant economic implications in traction drive systems.**

***Index Terms*—Fault diagnosis, fault tolerance, switched reluctance motor (SRM), traction motor drive.**

Nomenclature

D	PWM duty cycle.
i_a, i_b, i_c	Currents for phases A, B, and C.
$i'_{\max}$	Phase current peak when faulty.
$i_{\max}$	Phase current peak when normal.
Δi	Hysteresis window.
N_r	Rotor poles.
K_L	Inductance slope when normal.
K'_i	Current slope when normal.
K'_L	Inductance slope when faulty.
K_i	Current slope when faulty.
$L_{\min}$	Minimum of the phase inductance.
$L_{\max}$	Maximum of the phase inductance.
T^*	Given load torque.
T	Instantaneous torque.
$T_{\rm av}$	Average electromagnetic torque of one phase when normal.
$T'_{\rm av}$	Average electromagnetic torque of one phase when faulty.
$V_{\rm dc}$	Bus voltage.
ω_r	Angular velocity.
$\theta_{\rm on}$	Turn-on angle.
$\theta_{\rm off}$	Turn-off angle.
$R_{\rm eq}$	Equivalent resistance of loop.
θ_p	Phase current ending angle.
$i_s(\theta)$	Instantaneous phase current.

Manuscript received June 3, 2015; revised August 13, 2015 and August 23, 2015; accepted August 24, 2015. Date of publication September 7, 2015; date of current version January 7, 2016. This work was supported by the Engineering and Physical Sciences Research Council of UK (EP/L00089X/1) and National Natural Science Foundation of China under Grant 51361130150. Recommended for publication by Associate Editor J. A. Pomilio.

Y. Hu is with the College of Electrical Engineering, Zhejiang University, Hangzhou 310027, China, and also also with the Department of Electronic and Electrical Engineering, University of Strathclyde, Glasgow G1 1XQ, U.K. (e-mail: yihua.hu@strath.ac.uk).

C. Gan and W. Li are with the College of Electrical Engineering, Zhejiang University, Hangzhou 310027, China (e-mail: ganchun.cumt@163.com; woohualee@zju.edu.cn).

W. Cao is with the School of Electronics, Electrical Engineering and Computer Science, Queen's University Belfast, Belfast BT7 1NN, U.K. (e-mail: wencao@mit.edu).

J. Zhang and S. Finney are with the Department of Electronic and Electrical Engineering, University of Strathclyde, Glasgow G1 1XQ, U.K. (e-mail: jiangfeng.zhang@strath.ac.uk; stephen.finney@strath.ac.uk).

Color versions of one or more of the figures in this paper are available online at http://ieeexplore.ieee.org.

Digital Object Identifier 10.1109/TPEL.2015.2477165

I. Introduction

Over the recent decades, the development of electric vehicles (EVs) and hybrid electric vehicles (HEVs) is considered to be a key measure to reducing CO_2 emission and environmental pollution [1]–[5]. Switched reluctance motors (SRMs) are characterized with rare-earth-free and wide-speed-range advantages and are becoming an attractive technology for EV/HEV applications [6]–[12]. Due to the harsh operational environments and repetitive duty cycles, power electronic devices in traction drives are prone to failure in the transient of speed up and braking [13], [14]. Therefore, high reliability and fault tolerance are of critical importance in EV/HEV applications.

In SRM drives, the asymmetrical half-bridge topology is the most widely used converter topology. Its fault diagnosis (such as short circuit and open circuit) is researched in papers [15]–[21]. For example, paper [16] uses the bus current, paper [17] uses the freewheeling current, and paper [18] uses the phase current to distinguish open-circuit from short-circuit faults. Other analytical methods such as fast Fourier transformation, genetic-algorithm-based artificial neural network, and fuzzy logic are introduced in fault diagnosis [19]–[21]. The SRM fault is also studied in [22]–[24]. By injecting high-frequency pulses, the fault phase winding can be identified and the fault category also can be determined [24].

For the fault-tolerant SRM structure, increasing the number of phase in SRMs is a common method [25], [26]. Dual channels are also developed to improve the reliability of SRM-driving systems [27]. A modular stator structure is developed to bypass the fault winding [28], [29]. In [30], a double-layer-per-phase isolated SRM is proposed to improve the fault-tolerant capability.

TABLE I
COMPARISON OF FAULT-TOLERANT METHODS

Topology / Item	Traditional SRM system [18]	Specially designed motor [28][30]	Fault tolerance topology Paper [32]	Fault tolerance topology Paper [31]	Expected fault tolerance structure
Motor	Traditional SRM	Special design	Special design	Traditional SRM	Traditional SRM
Converter modular structure	Yes	Yes	Yes	No	Yes
Fault diagnosis	Complicated	N/A	Easy	N/A	Easy
Fault tolerant operation ability	Achievable with phase absence	Achievable with phase absence	Achievable without phase absence	Achievable with phase absence	Achievable without phase absence
Cost	Low	High	High	Medium	Low

The fault-tolerant converter topology for SRM drive systems is studied in [31] and [32]. In order to decrease the impact of faults on the drive performance, paper [31] proposes a new topology with two switching devices added to the traditional asymmetric half-bridge topology, while it is not in the modular structure. A decentralized topology is developed in [32] to make full use of independent phase windings, but a large number of power switching devices are needed. A three-phase bridge inverter is adopted in [33] and the corresponding fault-tolerant scheme is also developed. However, the converter cannot bypass the fault winding.

For fault-tolerant control, artificial neural network and genetic algorithm are developed [34]. The fuzzy logic control without a model is proposed in [35] to improve the performance of the SRM under fault conditions. In the absence of position sensors, a fault-tolerant control strategy is proposed in [36] to deal with the phase-absent operation. A traditional asymmetrical half-bridge topology can provide fault tolerance if the SRM drive is partially faulty with the absence phase operation. In case faults occur in all phases, the SRM drive will stop working. Paper [37] proposes a fault-tolerant topology with a modular structure. There is a single extra connection node per phase. In case a fault occurs, this fault-tolerant topology can only save 1/2 winding in the fault phase. Besides, it also requires three half-bridge legs for the fault-tolerant operation. A comparison of the fault-tolerant methods is illustrated in Table I. It can be seen that the current strategies can provide some fault-tolerant functions.

In order to satisfy the application requirements, the fault-tolerant SRM drive system should require the following conditions: 1) no change in the traditional SRM structure; 2) easy to fault diagnosis; 3) adapt to all kinds of converter and phase-winding faults; 4) a fault-tolerant topology with a module structure that suits for massive production; 5) relative low cost; and 6) adapt to both three-phase SRM and four-phase SRM drive systems. This paper is set out to develop a highly fault-tolerant SRM drive with the flexible converter topology to match the above conditions. In Section II, the proposed fault-diagnosis topology and strategy are introduced. In Section III, the fault-tolerant operation control strategy is illustrated. The popularization and application of the proposed method are presented in Section IV. Simulation and experiment are given in Section V. Section VI presents the conclusion.

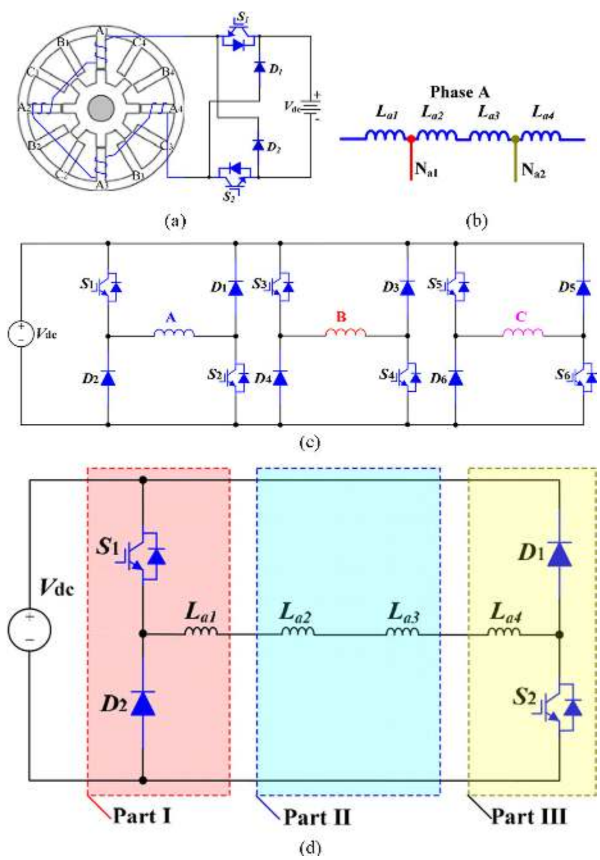

Fig. 1. Basic winding structure and driving topology of a 12/8 SRM. (a) Phase converter of 12/8 SRM. (b) Phase-winding tapping node. (c) 12/8 driving topology. (d) Three components of each phase converter.

II. FAULT-DIAGNOSIS TOPOLOGY AND STRATEGY

A new fault-tolerant topology is developed to improve the system performance that can also improve SRM-driving system fault-tolerant ability.

A. Proposed Fault-Tolerant Topology

Traditionally, for a three-phase 12-slot/8-pole (12/8) SRM, each phase is composed of four series-connected windings, as shown in Fig. 1(a). For phase A, the connection nodes for four winding are marked as N_{a1} and N_{a2}, as presented in Fig. 1(b).

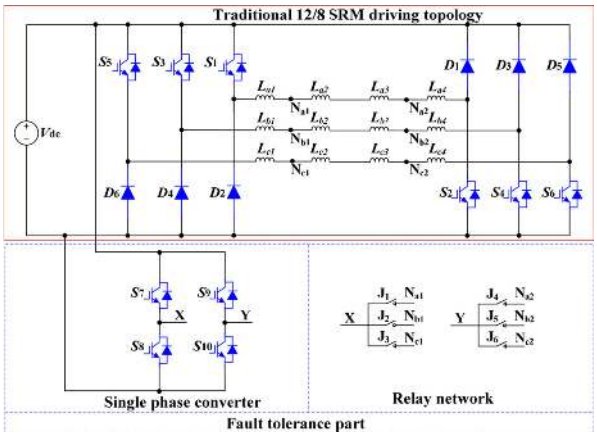

Fig. 2. Fault-tolerant topology for a 12/8 SRM.

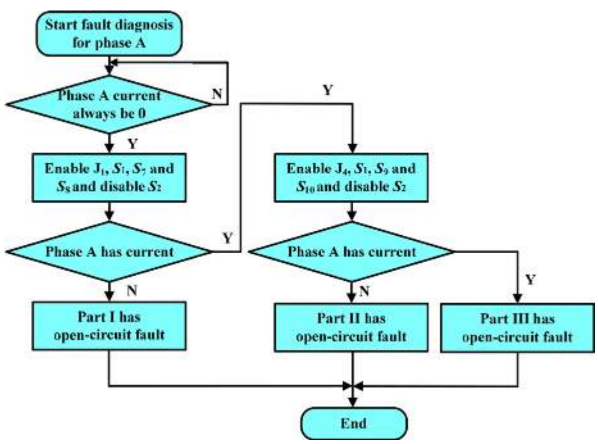

Fig. 3. Flowchart of the open-circuit fault diagnosis.

The asymmetrical half bridge is employed as the driving topology, as shown in Fig. 1(c). In Fig. 1(c), S_1, S_3, and S_5 are upper switching devices, and S_2, S_4, and S_6 are lower switching devices; $D_1 - D_6$ are freewheeling diodes. In order to locate the fault position precisely, each phase converter is divided into three parts (I–III), as illustrated in Fig. 1(d). The proposed fault-tolerant topology is presented in Fig. 2.

B. Open-Circuit Fault Diagnosis

Open-circuit faults are common fault phenomena in the SRM-driving system. In the traditional asymmetrical half-bridge topology, when an open-circuit fault occurs in a phase converter, the corresponding phase is out of operation, and the SRM will work in a phase absence operation. The machine torque becomes unbalanced and the torque ripple is increased. The signature of such a fault is zero current in a phase converter, which is easy to pick for diagnosis purposes. In order to achieve fault-tolerant operation, the fault part of the phase converter should be located. The flowchart of single-phase open-circuit diagnosis is shown in Fig. 3. First, the diagnosis system checks if the phase current is always zero. If this is the case, the system takes the following actions: J_1 is switched ON and S_2 is switched OFF. Then, the controller gives driving signal to S_1, S_7, and S_8. If the phase A converter can operate, part I is healthy; otherwise, part I is faulty. Next, switching ON J_4 and giving the signal of S_1, S_9, and S_{10}, if the phase A can still operate, part II is healthy and part III is unhealthy; otherwise, part II is unhealthy and part III is healthy. When multiphase fault occurs, the fault diagnosis is carried out phase by phase; each phase fault-diagnosis progress is the same as in Fig. 3 with enabling corresponding relays and switching devices.

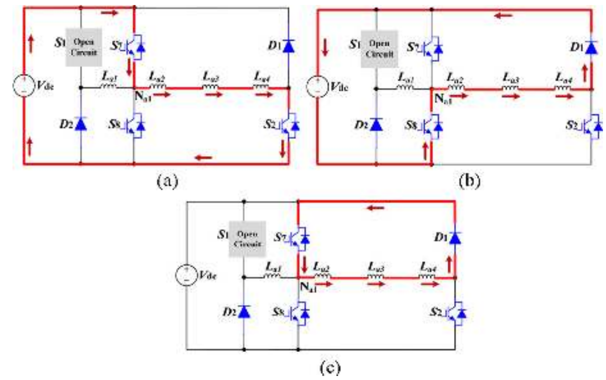

Fig. 4. Working states under part I fault conditions. (a) Excitation state. (b) Energy recycling state. (c) Freewheeling conduction state.

C. Fault-Tolerant Operation Under Open-Circuit Fault Conditions

Due to the central symmetry of the phase converter, there are two kinds of fault-tolerant operation modes. The first one is part I and part III fault scenario and the other is part II fault scenario.

When part I is under the fault condition, by turning ON relay J_1, the fault-tolerant bridge arm (composed of S_7 and S_8) and the healthy parts form a new topology; the corresponding working states are presented in Fig. 4(a)–(c). In the newly formed fault-tolerant operation topology, when S_7 and S_2 conduct, the excitation circuit is shown in Fig. 4(a). Fig. 4(b) presents the energy recycling mode, in which the winding voltage is $-V_{\mathrm{dc}}$ to speed up winding demagnetization. Fig. 4(c) shows the freewheeling conduction mode, in which the winding L_{a2}, L_{a3}, and L_{a4} voltage is 0. Similarly, when part III is under the fault condition, by switching ON relay J_4, the fault-tolerant bridge arm (composed of S_9 and S_{10}) and the healthy parts form a new topology to sustain operation.

When part II is under the fault condition, switching ON relay J_1 and J_4, the bridge arm composed of S_7 and S_8 and part I form one topology; the bridge arm composed of S_9 and S_{10} and part III form another topology. Two topologies work together to decrease the influence of part II open circuit. The corresponding working states are presented in Fig. 5(a)–(c).

When multiple phases have faults at the different parts, as shown in Fig. 6, part I of phase A and part III of phase B are in open-circuit fault condition. Switching ON relay J_1, the bridge arm composed of S_7 and S_8 is employed by phase A to form a new topology to realize fault-tolerant operation of phase A; switching ON relay J_5, the bridge arm composed of S_9 and S_{10} is employed by phase B to form a new topology to realize fault-tolerant operation of phase B. The corresponding working states are presented in Fig. 6(a)–(f). Fig. 6(a)–(c) shows three

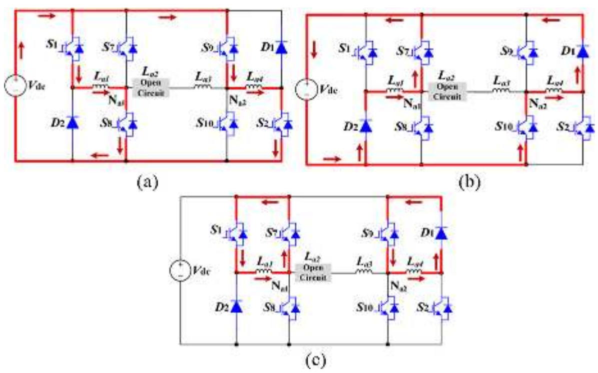

Fig. 5. Working states under part II fault conditions. (a) Excitation state. (b) Energy recycling state. (c) Freewheeling conduction state.

working states of phase A; Fig. 6(d)–(f) shows three working states of phase B.

The proposed fault-tolerant strategy can also operate in different winding open-circuit fault conditions. When L_{a1}, L_{b1}, and L_{c1} are open-circuited, as shown in Fig. 7(a), by enabling relay J_1, J_2, and J_3, the bridge arm composed of S_7 and S_8 is employed by phases A, B, and C to form a new topology to realized fault-tolerant operation, in which S_7 is with the function of public switching devices. The other fault scenario is different part in different phases, as shown in Fig. 7(b); by enabling relay J_1, J_3, J_5, and J_6, both half-bridge arms are employed by phases A, B, and C to form a new topology to realized fault-tolerant operation. For phase A, S_7, S_8, D_1, and S_2 form a new driving topology; for phase B, S_3, D_4, S_9, and S_{10} form a new topology; for phase C, S_7, S_8, S_9, and S_{10} form a new topology.

D. Switching Device Short-Circuit Fault Diagnosis

Switching device short circuit and inner-turn short circuit are the two causes for short-circuit faults. For the inner-turn short circuit, the phase windings can still operate; nevertheless, when the converter is under switching device short-circuit fault condition, the freewheeling current cannot decrease to zero after turning OFF switching devices of the phase converter, which leads to negative torque that influence the SRM system operation. When the upper switching device of phase A is short-circuited, the only freewheeling mode is illustrated in Fig. 8(a); when the lower switching device of phase A is short-circuited, the only freewheeling mode is illustrated in Fig. 8(b). As illustrated in Fig. 8, because there is no energy recycling loop, the corresponding phase current is always higher than zero that can be employed in short-circuit fault diagnosis. Fig. 8(c) shows a flowchart of the diagnosis of switching device short circuits. When the phase current is always higher than zero, the corresponding phase is short-circuited. After enabling J_4, S_1, S_9, and S_{10} to form a new converter and if the phase current decreases to zero, S_2 is proven to be short-circuited. If the phase current is still higher than zero, S_1 is short-circuited.

E. Fault-Tolerant Operation Under Hybrid Fault Conditions

When the SRM traditional asymmetrical half-bridge topology is under hybrid fault conditions, in which both open circuit and

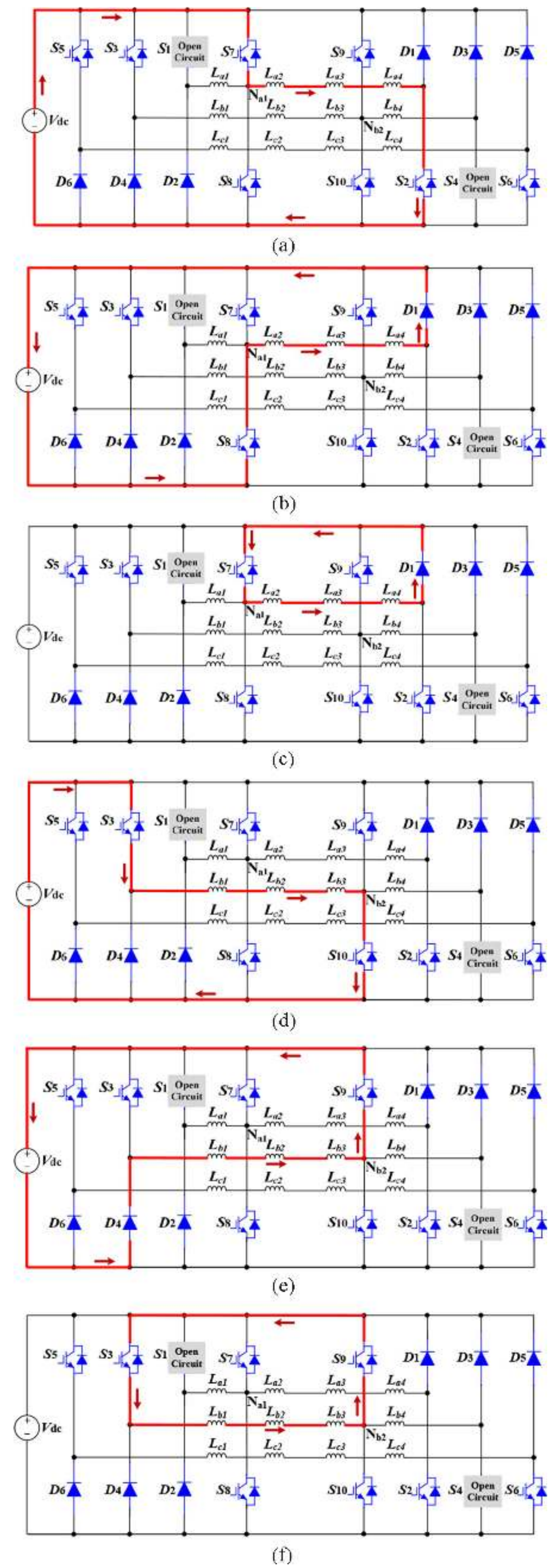

Fig. 6. Working states under multiphase part I fault condition. (a) Excitation state of phase A. (b) Energy recycling state of phase A. (c) Freewheeling conduction state of phase A. (d) Excitation State of phase B. (e) Energy recycling state of phase B. (f) Freewheeling conduction state of phase B.

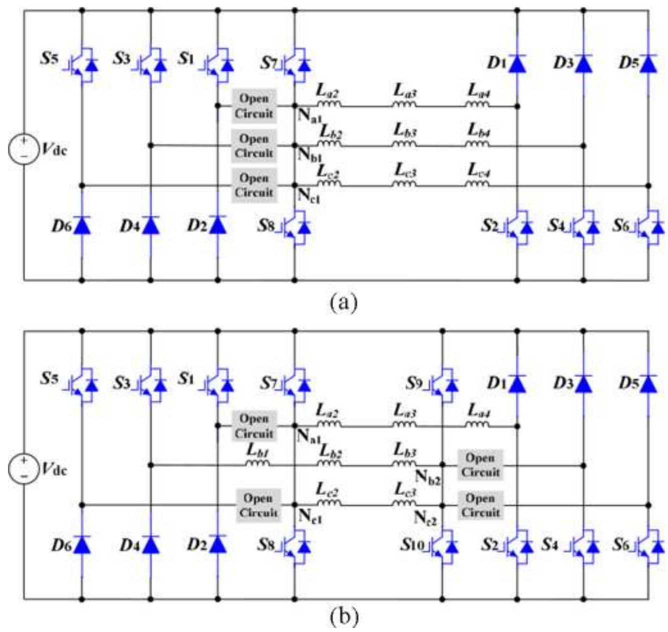

Fig. 7. Open-circuit fault scenario in windings. (a) Open circuit in three phases in same part. (b) Open circuit in three phases in different part.

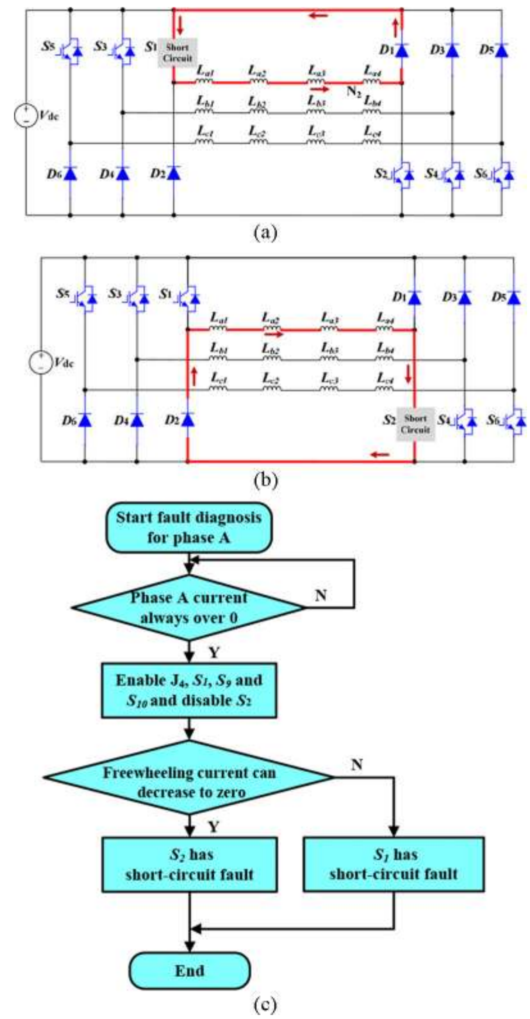

Fig. 8. Fault diagnosis and tolerance under switching device short-circuit faults. (a) Upper switching device short circuit. (b) Lower switching device short circuit. (c) Flowchart for the diagnosis of the switching device short circuits.

short circuit occur in the traditional topology, the fault-tolerant part can help SRM to achieve fault-tolerant operation. Fig. 9(a) presents the scenario of all upper switching devices which are under the fault condition, in which S_1 and S_3 are under the short-circuit fault condition and S_5 is under the open-circuit fault condition; the traditional topology cannot work under the fault condition of Fig. 9(a). In the proposed fault-tolerant topology, the relay J_1, J_2, and J_3 are switched ON, and the bridge arm composed of S_7 and S_8 is activated to form a new topology, as shown in Fig. 9(b). In the new topology, the fault part of each phase is blocked; the S_7 is acted as public switching devices, and the three phases all can operate, in which only 1/4 part of phase winding cannot output torque. Fig. 9(c) shows the hybrid fault scenario 2, in which the upper switching device S_1 is under short-circuit fault, the upper switching device S_5 is under open-circuit fault, and the lower switching device S_4 is under short-circuit fault condition. Switching ON J_1 and J_3 and activating S_7 and S_8, faulty S_1 and S_5 can be blocked; switching ON J_5 and activating S_9 and S_{10}, faulty S_4 can be blocked; the fault-tolerant state is presented in Fig. 9(d). Fig. 9(e) shows the hybrid fault scenario 3, in which fault occurs at different phases and different parts. Switching ON J_1, J_3, J_4, and J_5, a single-phase bridge is activated, as presented in Fig. 9(f).

F. Fault-Tolerant Topology Formation Rule

In order to maintain phase independence, when part II of each phase converter is healthy, two phase nodes all connected to bridge arms are not allowed. When part II of the phase converter is faulty, the corresponding fault phase can be connected to both bridge arms without influence of other phase. As shown in Fig. 10, although J_1, J_2, J_4, and J_5 are switched ON, L_{a2} is open-circuited such that there is no loop in part windings of phase A (L_{a2} and L_{a3}) and part windings of phase B (L_{b2} and L_{b3}).

There are only two bridge arms in the fault-tolerant part. Due to the traditional topology central symmetry, one bridge arm can block part I fault of the phase converter and the other bridge arm can block part III fault of the phase converter; when part II phase converter is under open-circuit condition, both bridge arms arm can support the corresponding fault phase to achieve fault-tolerant operation, as shown in Fig. 5. Therefore, the two bridge arms can support all kinds of fault-tolerant operation. The extremely fault condition is shown in Fig. 11; the shadow part of the converter is broken and only part II of phase A converter is healthy. By the proposed fault-tolerant topology, the SRM can still operate by the converter formed by single-phase bridge and phase winding L_{a2} and L_{a3}.

III. Fault-Tolerant Operation Control Strategy

Because the fault-tolerant topology and phase-winding node connection are developed, the corresponding control strategy,

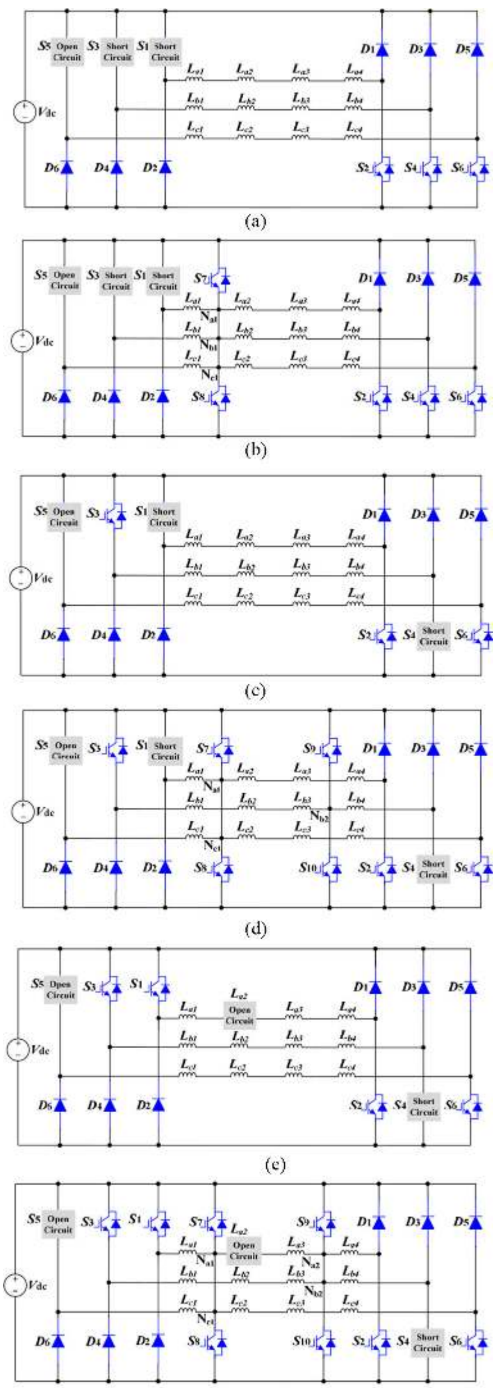

Fig. 9. Hybrid fault scenarios. (a) Hybrid fault scenario 1. (b) fault-tolerant state under hybrid fault scenario 1. (c) Hybrid fault scenario 2. (d) Fault-tolerant state under hybrid fault scenario 2. (e) Hybrid fault scenario 3. (f) Fault-tolerant state under hybrid fault scenario 3.

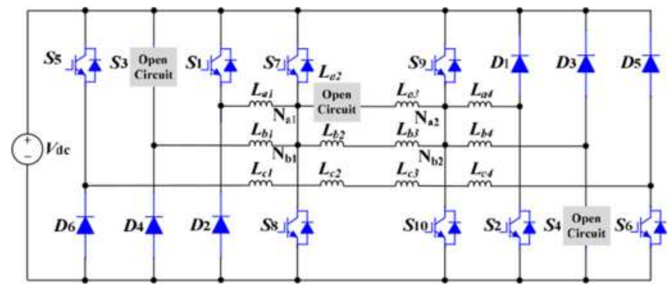

Fig. 10. Part II fault, node connection.

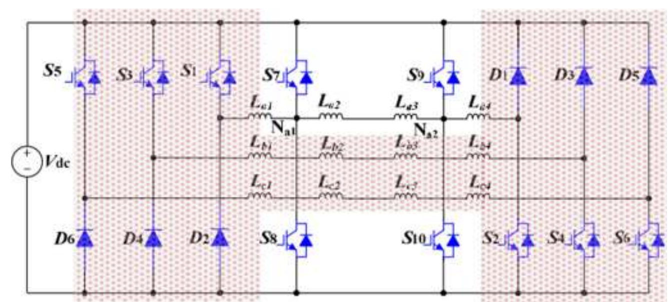

Fig. 11. Extreme fault-tolerant operation condition.

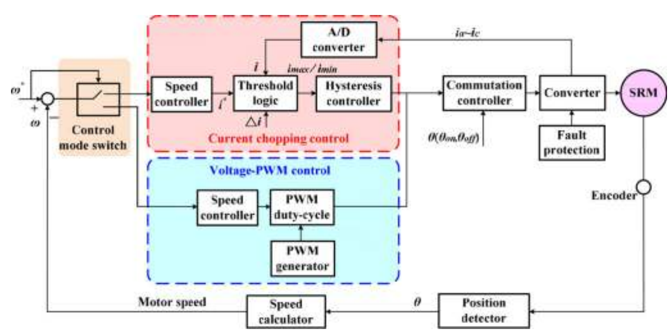

Fig. 12. SRM control strategy under healthy condition.

especially fault-tolerant operation, is needed to deal with the fault condition.

A. *Control Schemes for SRM Drives Under Healthy Condition*

When the SRM-driving system is in healthy condition, the fault-tolerant topology stays in the idle mode, and the system is the same as the traditional asymmetrical half-bridge topology; the current chopping control (CCC) and voltage-PWM control are employed as two basic schemes. According to the given speed ω^*, the CCC is activated at low-speed condition, while voltage-PWM control is activated at high-speed condition, as illustrated in Fig. 12. The speed controller (e.g., proportional-integral (PI) controller) is used to regulate the motor speed. The motor speed is measured by an encoder. The turn-on and turn-off angles are determined by a commutation controller. The fault protection is provided to deal with switching devices faults and phase-winding faults and so forth. In the CCC system, the phase current is addressed by a current controller. The current reference i^* is derived from the speed controller. The instantaneous phase currents are measured by current sensors and fed back to the threshold logic to calculate $i_{\max}$ and $i_{\min}$ that determine the switching states in each phase turn-on region. In the voltage-PWM control system, the phase voltage is addressed by a voltage controller. The PWM duty cycle is derived from the speed controller and regulated according to the instantaneous speed. The average voltage applied to the phase winding is chopped down to the value $DV_{\rm dc}$ with a duty cycle *D*.

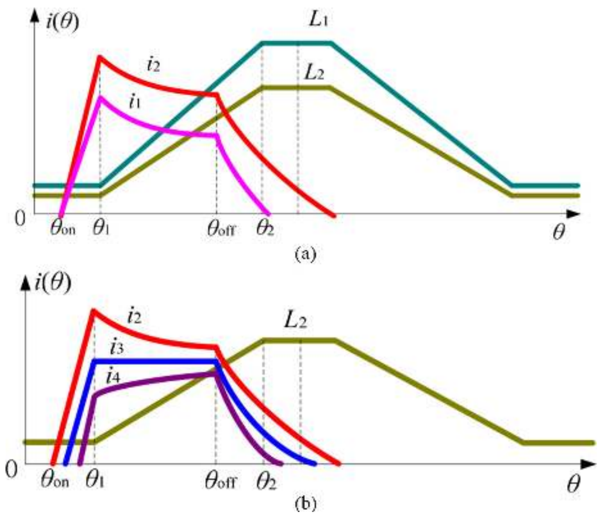

Fig. 13. Relationship between the phase current and phase inductance under part I fault condition. (a) Fault-tolerant operation with 3/4 phase winding. (b) Turn-on angle lagging behind.

B. Fault-Tolerant Control Under Unhealthy Conditions

When part I or part III of the traditional asymmetrical half-bridge topology is under the fault condition, the fault-tolerant topology can be formed by switching ON corresponding fault-tolerant part. In this process, the faulty part can be blocked, and the healthy part can still work.

Fig. 13 illustrates the relationship between the phase current, phase inductance, and rotor position. In the figure, $\theta_{\rm on}$ and $\theta_{\rm off}$ are the turn-on and turn-off angles, respectively, i_1 and L_1 are the phase current and phase inductance in normal conditions, respectively, i_2 and L_2 are the phase current and phase inductance in fault tolerance under part I fault conditions, respectively, and i_3 and i_4 are the phase currents when the turn-on angle is set lagged. Fig. 13(a) presents the phase current and phase inductance in the fault-tolerant operation with 3/4 phase winding. Due to the decrease of phase inductance under the fault condition, the phase current has higher current amplitude. Under the fault condition, by controlling the turn-on angle, the phase current can also be controlled as in the normal condition. The corresponding phase current is shown in Fig. 13(b). The waveforms are similar to that in the faulty case in part III.

The phase inductance slope in the inductance-ascending region is given by

$$K_L = \frac{L_{\max} - L_{\min}}{\theta_2 - \theta_1} \tag{1}$$

where $L_{\min}$ and $L_{\max}$ are the minimum and maximum of the phase inductance, respectively, and θ_1 and θ_2 are the relevant rotor positions.

In the region of $\theta_{\rm on} \le \theta < \theta_1$, the phase current is expressed as

$$i\,(\theta) = \frac{\theta - \theta_{\rm on}}{\omega_r \cdot L_{\min}} V_{\rm dc} \tag{2}$$

where $V_{\rm dc}$ is the bus voltage and ω_r is the rotor angular velocity. The phase current increases quickly in this region and the current slope factor K_i satisfies

$$K_i = \frac{di}{d\theta} = \frac{V_{\rm dc}}{\omega_r L_{\min}} > 0. \tag{3}$$

In the region of $\theta_1 \le \theta < \theta_{\rm off}$, the phase current is expressed as

$$i\,(\theta) = \frac{V_{\rm dc}}{\omega_r} \frac{\theta - \theta_{\rm on}}{L_{\min} + K_L\,(\theta - \theta_1)}. \tag{4}$$

The peak of the phase current is at θ_1 and can be written as

$$i_{\max} = \frac{\theta_1 - \theta_{\rm on}}{\omega_r \cdot L_{\min}} V_{\rm dc}. \tag{5}$$

The average electromagnetic torque of one phase can be expressed as

$$T_{\rm av} = \frac{N_r}{2\pi} \frac{V_{\rm dc}^2}{\omega_r^2} (\theta_{\rm off} - \theta_1) \left(\frac{\theta_1 - \theta_{\rm on}}{L_{\min}} - \frac{1}{2} \frac{\theta_{\rm off} - \theta_1}{L_{\max} - L_{\min}} \right) \tag{6}$$

where N_r is the number of rotor poles.

If the SRM system has an open-circuit or short-circuit fault in part I or part III of the converter, the proposed fault-tolerant converter will operate with 3/4 part of the fault phase winding, and the new phase inductance can be expressed as

$$\begin{cases} L'_{\max} = \dfrac{3}{4} L_{\max} \\ L'_{\min} = \dfrac{3}{4} L_{\min} \end{cases} \tag{7}$$

where $L'_{\min}$ and $L'_{\max}$ are the minimum and maximum of the phase inductance in fault-tolerant operation, respectively.

In the inductance ascending region, the phase inductance slope can be expressed as

$$K'_L = \frac{3}{4} \frac{L'_{\max} - L'_{\min}}{\beta_s} = \frac{3}{4} K_L. \tag{8}$$

In the region of $\theta_{\rm on} \le \theta < \theta_1$, the phase current slope in the fault-tolerant operation is given by

$$K'_i = \left(\frac{di}{d\theta} \right)' = \frac{V_{\rm dc}}{\omega_r \frac{3}{4} L_{\min}} = \frac{4V_{\rm dc}}{3\omega_r L_{\min}} = \frac{4}{3} K_i. \tag{9}$$

In the fault-tolerant operation, at position $\theta = \theta_1$, the peak of the phase current can be written as

$$i'_{\max} = \frac{V_{\rm dc}}{\omega_r} \frac{\theta_1 - \theta_{\rm on}}{\frac{3}{4} L_{\min}} = \frac{V_{\rm dc}}{\omega_r} \frac{4(\theta_1 - \theta_{\rm on})}{3L_{\min}} = \frac{4}{3} i_{\max}. \tag{10}$$

The average electromagnetic torque is expressed as

$$T'_{\rm av} = \frac{N_r}{2\pi} \frac{V_{\rm dc}^2}{\omega_r^2} (\theta_{\rm off} - \theta_1) \left(\frac{\theta_1 - \theta_{\rm on}}{\frac{3}{4} L_{\min}} - \frac{1}{2} \cdot \frac{\theta_{\rm off} - \theta_1}{\frac{3}{4} L_{\max} - \frac{3}{4} L_{\min}} \right)$$
$$= \frac{4}{3} T_{\rm av}. \tag{11}$$

Clearly, the peak of the phase current and the average electromagnetic torque of the failure phase are 4/3 of the normal value when working in the fault-tolerant operation.

If the voltage drop that is caused by winding resistance and solid state devices is considered, (11) can be revised as

$$T''_{\mathrm{av}} = \frac{N_r}{2\pi} \frac{V_{\mathrm{dc}}^2 [1 - R_{\mathrm{eq}} \sqrt{\frac{N_r}{2\pi} \int_{\theta_{\mathrm{on}}}^{\theta_p} i_s^2(\theta)}]^2}{\omega_r^2} (\theta_{\mathrm{off}} - \theta_1) \left(\frac{\theta_1 - \theta_{\mathrm{on}}}{\frac{3}{4} L_{\min}} - \frac{1}{2} \cdot \frac{\theta_{\mathrm{off}} - \theta_1}{\frac{3}{4} L_{\max} - \frac{3}{4} L_{\min}} \right) \quad (12)$$

where R_{eq} is the equivalent resistance of loop, θ_p is the phase current ending angle, and $i_s(\theta)$ is the instantaneous phase current.

When part I or III is faulty, considering the proposed fault-tolerant scheme in a CCC system, 3/4 part of the failure phase can still work to output torque. Although 1/4 part of the failure phase is out of operation and the phase current is the control reference, it will be regulated to the same reference with the normal condition. In the voltage-PWM control system, the phase voltage is employed as a control reference and the imposed voltage on each phase is the same. The current in the fault phase will be larger than that in other healthy phases due to the decreased phase inductance. In order to further reduce the unbalanced phase current in the voltage-PWM system, the turn-on angle of the failure phase can be used to adjust lagging to reduce the increased phase current in the failure winding, as illustrated in Fig. 13(b). Therefore, the proposed fault-tolerant technology can be employed to compensate the current and torque and reduce the torque ripple to improve the drive performance in fault conditions.

IV. Popularization and Application

In addition to three-phase 12/8 SRM-driving systems, four-phase eight-slot/six-pole (8/6) SRM-driving systems are also widely used. The proposed fault tolerance can also be used in four-phase 8/6 SRM.

A. Fault-Tolerant Topology for Four-Phase 8/6 SRM

Traditionally, for the 8/6 SRM, each phase is composed of two winding series connection, as shown in Fig. 14(a); for phase A, the connection node for two winding is marked as N_a, and the phase converter is divided into two parts, left part and right part, as presented in Fig. 14(b). The proposed fault-tolerant topology is illustrated in Fig. 14(c), which is composed of a signal-phase converter and a relay network.

B. Fault-Tolerant Operation

Because the traditional 8/6 converter is composed of two parts, usually, the fault can occur in either. The bridge arm composed of S_9 and S_{10} can block the left-part fault, and the bridge arm composed of S_{11} and S_{12} can block the right-part fault. The fault-diagnosis process is similar to the 12/8 SRM-driving system. Thanks to the relay network, when the faulty part is located in the fault phase, the corresponding relay is switched ON to block the faulty part. Fig. 15 shows the typical hybrid faulty scenario in which each phase has fault; in the traditional 8/6 SRM topology, the driving system cannot work. By the proposed fault-tolerant topology, the faulty 8/6 SRM

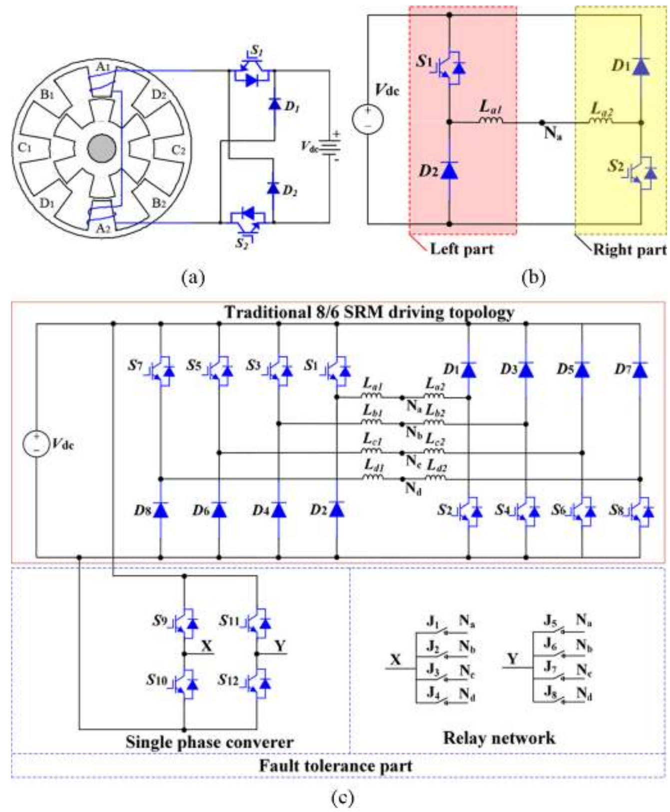

Fig. 14. Fault tolerance topology for the 12/8 SRM. (a) Phase converter of 8/6 SRM. (b) Phase converter with winding central tapping node. (c) Proposed fault-tolerant topology.

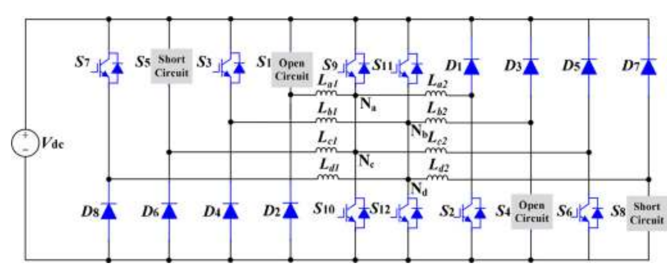

Fig. 15. Fault-tolerant topology under hybrid fault scenario for the 8/6 SRM.

can still operate with the new formed phase converter avoiding phase absence operation, and the states of phase windings in relation to the switching actions are illustrated in Table II.

V. Simulation and Experiment

In order to validate the proposed fault-tolerant topology, a 750-W 12/8 SRM is modeled in the MATLAB/Simulation. Fig. 16 presents the simulation results of the 12/8 SRM in the voltage-PWM control mode at 600 r/min under normal and fault conditions. The turn-on and turn-off angles are set to 0° and 20°, respectively; the load torque is set to 1 N·m. In the waveforms, i_a, i_b, and i_c are the phase A, B, and C current, respectively. T and T^* are the instantaneous torque and given load torque, respectively. In the normal conditions, the three phase currents have the same shape with 15° phase-shift compared to each

TABLE II
RELATIONSHIP OF WORKING PHASE WITH SWITCHING DEVICES

Working phase	Conducting device	State of Phase
Phase A	S_9, S_2	Excitation
	S_{10}, D_1	Demagnetization
Phase B	S_3, S_{12}	Excitation
	D_4, S_{11}	Demagnetization
Phase C	S_9, S_6	Excitation
	S_{10}, D_5	Demagnetization
Phase D	S_7, S_{12}	Excitation
	D_8, S_{11}	Demagnetization

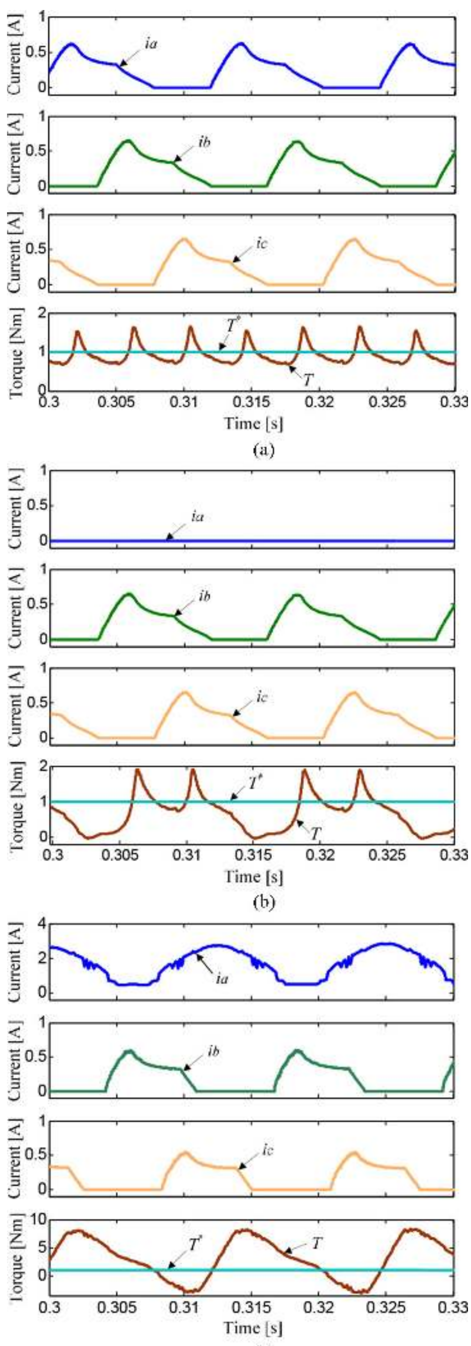

Fig. 16. Simulation results of the 12/8 SRM in voltage-PWM control mode under normal and fault conditions. (a) Normal condition. (b) Open-circuit fault of part I. (c) Short-circuit fault of part I.

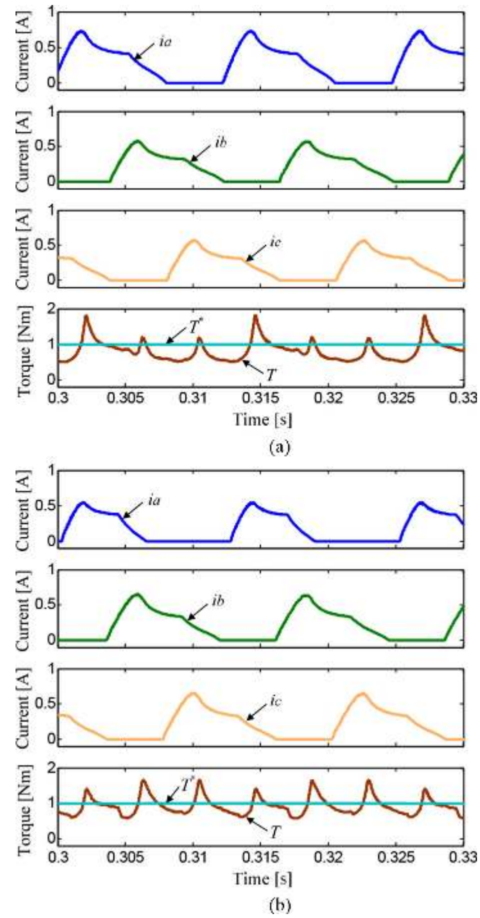

Fig. 17. Simulation results of the 12/8 SRM in voltage-PWM control mode with fault-tolerant topology under fault conditions. (a) Turn-on angle is 0° for phase A. (b) Turn-on angle is 5° for phase A.

other, and the total torque is the sum of three phase torque, as shown in Fig. 16(a). Fig. 16(b) shows the simulation results of switching device open-circuit fault condition of part I; thanks to the independence of each phase leg, the fault phase will not affect the other healthy phase, while the torque ripple gets larger than that in normal conditions. Fig. 16(c) shows the simulation results of upper switching device short-circuit fault condition of phase A; the corresponding phase voltage cannot be regulated in phase turn-on region, and the demagnetization current also cannot flow to power supply in the phase turn-off region; therefore, phase A current is obviously larger than the normal phase, causing the torque ripple.

Fig. 17 illustrates the simulation results of the 12/8 SRM in the voltage-PWM control mode at 600 r/min with the fault-tolerant topology under phase A fault conditions. In Fig. 17(a), the current slope and peak value of phase A in the initial conduction region are 4/3 of the normal value that coincides with theory analysis, although using the fault-tolerant topology, the torque ripple is still large. In order to reduce torque ripple effectively, a fault-tolerant scheme lagging the turn-on angle of the fault phase is carried out, as presented in Fig. 17(b). The turn-on angle is set to 5° for phase A, and the torque ripple is clearly reduced compared to Fig. 17(a).

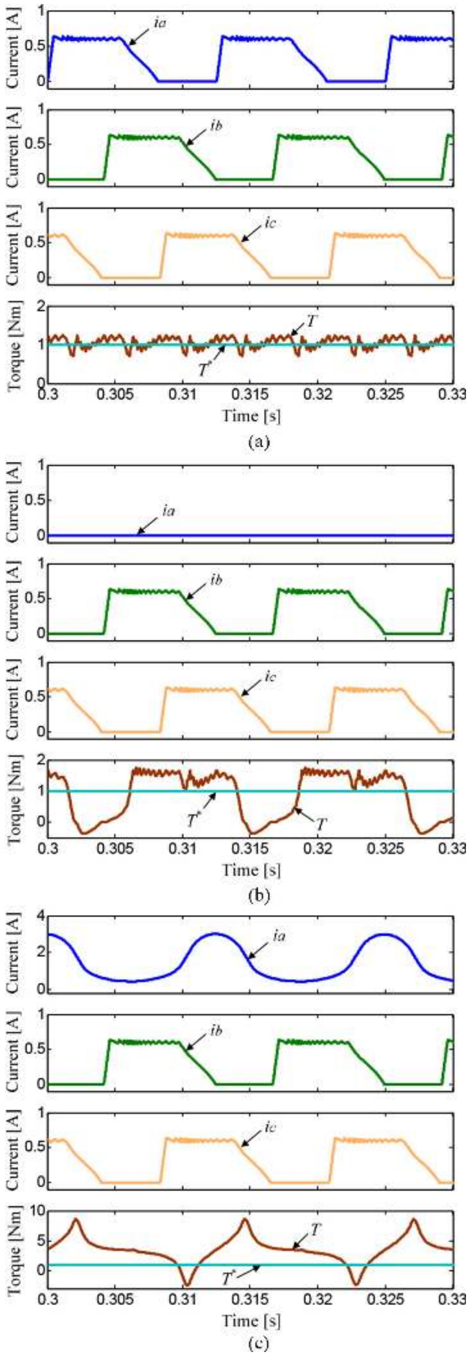

Fig. 18. Simulation results of the 12/8 SRM in current regulation control mode with fault-tolerant topology under fault conditions. (a) Normal. (b) Open-circuit fault. (c) Short-circuit fault.

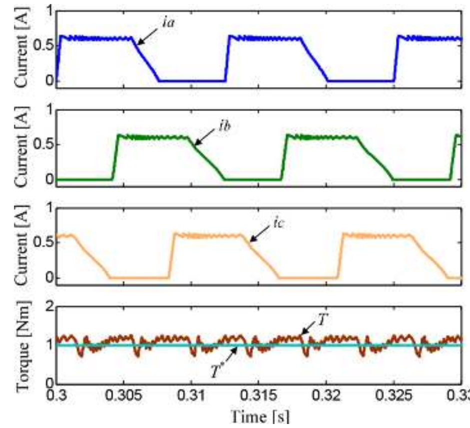

Fig. 19. Simulation results of the 12/8 SRM in CCC mode with fault-tolerant topology under fault conditions.

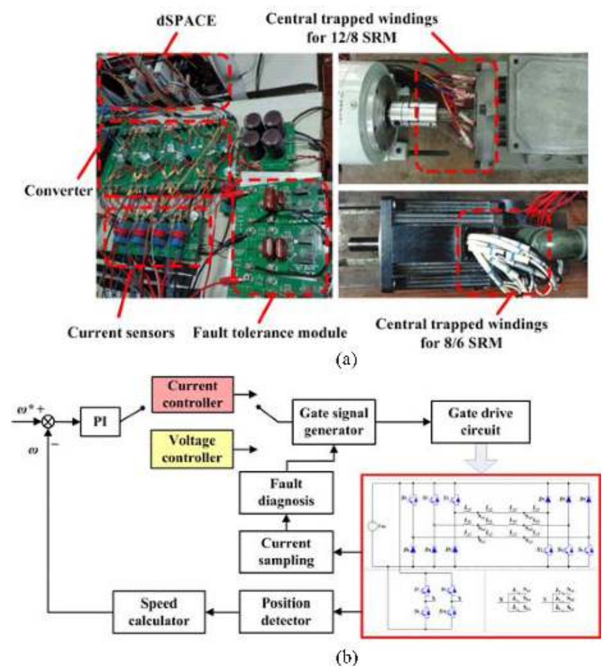

Fig. 20. Experimental setup and the control system. (a) Experimental setup. (b) Diagram of the fault-tolerant control system.

Fig. 18 illustrates the simulation results of the 12/8 SRM in the CCC mode under normal and fault conditions, respectively. In Fig. 18(a), the torque ripple is smaller than that of the voltage-PWM control mode in the normal condition shown in Fig. 16(a). Fig. 18(b) and (c) shows the simulation results under open- and short-circuit fault conditions that are similar to the voltage-PWM control mode. Fig. 19 presents the fault-tolerant results in the current regulation control mode at 600 r/min with the proposed fault-tolerant topology. In the current regulation control system, phase current is the control target, and it is regulated to the same reference compared to the normal one, and the torque ripple is effectively reduced to the normal condition compared to Fig. 18(a).

To verify the effectiveness of the proposed fault-tolerant scheme, an experimental rig for testing a 12/8 and a 8/6 prototype SRM is set up, as shown in Fig. 20(a). The main motor parameters are illustrated in Table III. Air switches are adopted to emulate open-circuit and short-circuit faults. The winding nodes are created and pulled out at the terminals when producing the prototype motor. An asymmetrical converter is employed in the system to drive the SRM, and a single-phase converter is used to achieve the fault-diagnosis and fault-tolerance operation. The switches are MOSFET FDA59N30 and diodes are IDW75E60. The Hall current sensors (LA55Ps) are adopted to measure the

TABLE III
12/8 AND 8/6 SRM SYSTEM PARAMETERS

Parameters	Value for the 12/8 SRM	Value for the 8/6 SRM
Phase number	3	4
Number of stator poles	12	8
Number of rotor poles	8	6
Number of windings per phase	4	2
Rated speed (r/min)	1500	1500
Rated power (W)	750	150
Rated voltage (V)	200	132
Rated current (A)	3.6	1.1
Rated torque (N·m)	4.77	0.95
Phase resistance (Ω)	3.01	9.01
Minimum phase inductance (mH)	27.2	28.65
Maximum phase inductance (mH)	256.7	226.03
Rotor outer diameter (mm)	55	54
Rotor inner diameter (mm)	30	22
Stator outer diameter (mm)	102.5	102
Stator inner diameter (mm)	55.5	54.5
Core length (mm)	80	58
Stator arc angle (deg)	14	21
Rotor arc angle (deg)	16	24
Switching devices (MOSFET)	FDA59N30	
Diode	IDW75E60	

phase currents. A 1000-line incremental encoder is used to measure the rotor position. A dSPACE 1006 platform is employed to implement the control algorithm. A magnetic brake acts as the load with a torque of 1 N·m. The dc-link voltage is fixed to 48 V. The torque observed in the oscilloscope is obtained online by using the real-time phase currents and rotor position to look up for the torque value in a 3-D torque table that includes the T-i-θ characteristics [33], [34]. The torque data in the lookup table are measured by using a rotor-clamping device when supplying different steady currents to the motor windings in a rotor position that changes step by step. The output torque in the experimental waveforms is observed though a D/A converter. Fig. 20(b) shows the fault-tolerant control system diagram with the closed-loop speed regulation capability. As illustrated in the figure, a PI controller is employed to regulate the motor speed, and the proportional gain and integral gain are 0.05 and 0.5, respectively. The current controller and voltage controller are utilized to generate the drive signals to control the motor drive in different operation modes. The position detector and speed calculator are used to give the instantaneous speed for feedback control. The current sampling and fault-diagnosis schemes are employed to control the gate signals for the fault-tolerant topology to operate under fault conditions.

Figs. 21–24 present the experimental results of the 12/8 SRM at 600 r/min, and the turn-on and turn-off angles are set to 0° and 20° in the 12/8 SRM drive. In the voltage-PWM control system with the fault-tolerant topology, the turn-on angle is set to 5° to improve the phase current balance for the fault-tolerant performance when the short-circuit fault occurs. Fig. 21 presents the typical voltage-PWM control model waveforms of the SRM under normal, open-circuit fault, and short-circuit fault conditions, respectively. Fig. 21(a) shows the experimental waveform under normal condition; three phases have the same current amplitude and shape. Fig. 21(b) shows the experimental result under the open-circuit fault condition without the proposed fault-tolerant

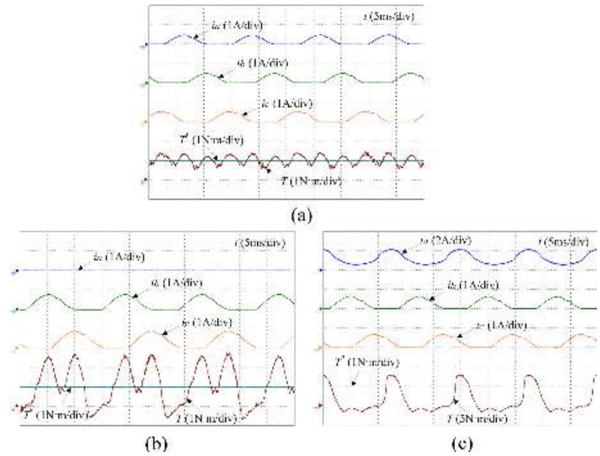

Fig. 21. Experimental results of the 12/8 SRM in voltage-PWM control mode under healthy and fault conditions. (a) Healthy condition. (b) Open-circuit fault of part I without fault-tolerant topology. (c) Short-circuit fault of part I without fault-tolerant topology.

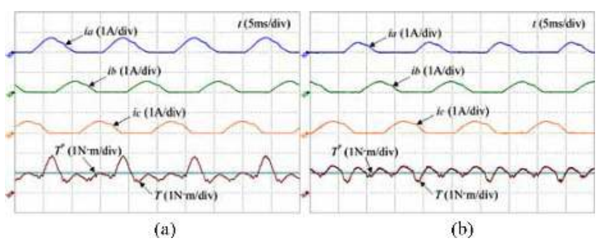

Fig. 22. Experimental results of the 12/8 SRM in voltage-PWM control mode with fault-tolerant topology under phase A fault conditions. (a) 0° turn-on angle for phase A. (b) 5° turn-on angle for phase A.

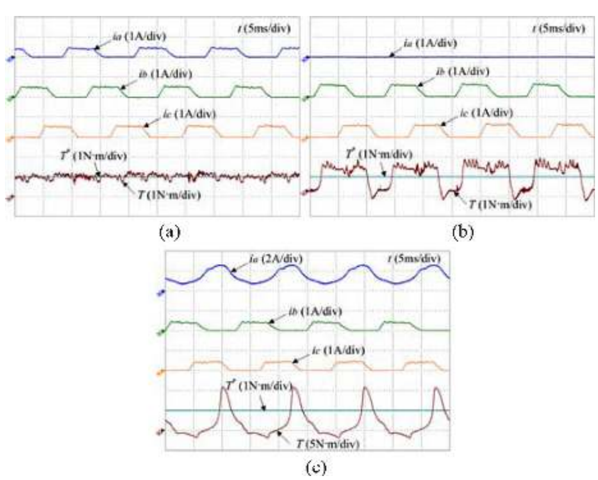

Fig. 23. Experimental results of the 12/8 SRM in CCC mode without fault-tolerant topology under phase A fault conditions. (a) Healthy. (b) Open-circuit fault of part I without fault-tolerant topology. (c) Short-circuit fault of part I without fault-tolerant topology.

strategy; there is no current in the fault phase; in a closed-loop system, when the open-circuit fault happens, the other two phase currents are excited to be larger than the previous one by increasing the PWM duty cycle, to compensate the absent phase torque. Fig. 21(c) presents the short-circuit fault condition without the

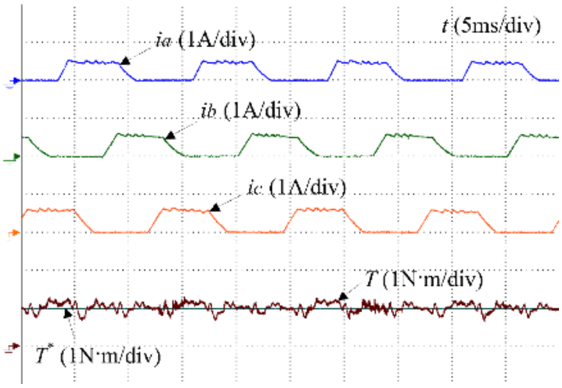

Fig. 24. Experimental results of the 12/8 SRM in CCC mode with fault-tolerant topology under phase A fault conditions.

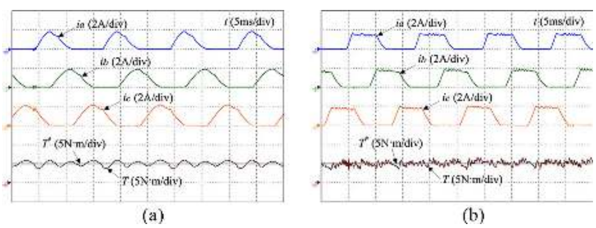

Fig. 25. Experimental results of the 12/8 SRM in fault-tolerant operation under the high load. (a) Voltage-PWM control mode. (b) CCC mode.

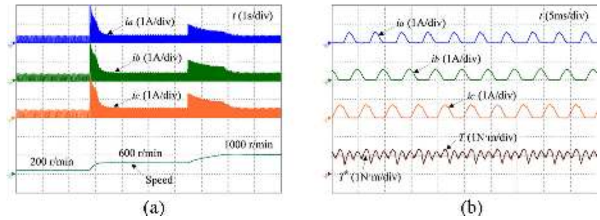

Fig. 26. Experimental results of the 12/8 SRM in fault-tolerant operation during acceleration. (a) Acceleration (b) Operation at 1500 r/min.

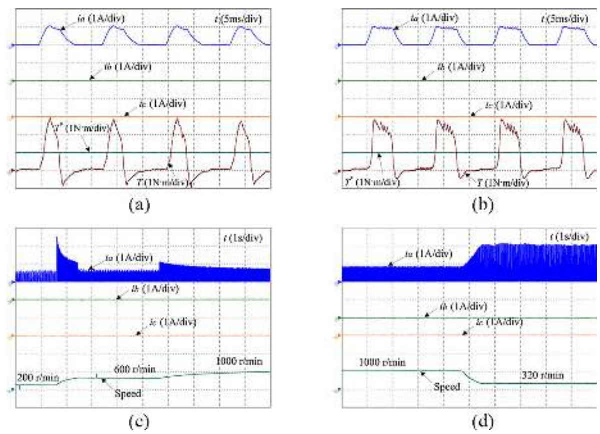

Fig. 27. Experimental results of the 12/8 SRM in fault-tolerant operation with only a half phase winding in the extreme fault condition at steady-state operation. (a) Voltage-PWM control mode. (b) CCC mode. (c) Acceleration. (d) Load increase.

proposed fault-tolerant strategy, in which the fault phase current cannot decrease to zero; the experiment results have agreed well with the analytical study in Section II. Fig. 22 verifies the control strategy in the voltage-PWM control mode under the fault condition. As shown in Fig. 22(a) and (b), by controlling the turn-on angle of the fault phase, the output torque ripple can be decreased obviously. Fig. 23 presents the typical waveforms for the CCC model under normal, open-circuit fault, and short-circuit fault condition. In the open-circuit fault condition, there is no current in the fault phase, as shown in Fig. 23(b), while in the short-circuit fault condition, the fault phase current cannot decrease to zero, as shown in Fig. 23(c). With the proposed fault-tolerant method, the fault phase current and output torque can follow the reference values faithfully under the CCC mode, as shown in Fig. 24. Due to the symmetrical structure of parts I and III of the phase converter [see Fig. 1(d)], part I fault has the same characteristics as part III fault.

Fig. 25 shows the fault-tolerant operation at 600 r/min and 5-N·m load in CCC and voltage-PWM control modes under phase A part I fault condition. The system can still be stable when operating at large load and make up for the missing output torque of the fault phase. Fig. 26 shows the operation of the developed system during acceleration and at high speed with the 1-N·m load. As illustrated in Fig. 26(a), the speed follows the given value well during the continuous acceleration progress. In Fig. 26(b), the system is still stable when it is operated at 1500 r/min, which presents good stability.

Fig. 27 shows the fault-tolerant operation with only a half-phase winding at 600 r/min and 1-N·m load in voltage-PWM control and CCC modes, respectively. As shown in Fig. 27, only phase A has current and the other phases are out of operation. The system can still operate with only a half-phase winding at light load. Fig. 27(c) and (d) illustrates the fault-tolerant operation with only a half-phase winding during acceleration and load increasing. The speed still follows the given speed well no matter during acceleration and in steady state, as shown in Fig. 27(c). However, in Fig. 27(d), when the load increases from 1 to 3 N·m, the speed is reduced due to the insufficient load ability. Hence, in the extreme fault conditions, the proposed fault-tolerant scheme can still operate at light loads.

In order to verify the proposed fault-tolerant scheme for the 8/6 SRM, the experimental tests are also carried out on a four-phase 8/6 SRM. Fig. 28 presents the operation waveforms under normal, open-circuit fault, and short-circuit fault conditions without the proposed fault-tolerant strategy. The turn-on and turn-off angles are set to 0° and 28°, respectively. Fig. 29 shows the experimental waveforms with the proposed fault-tolerant strategy. In the voltage-PWM control system with the fault-tolerant topology, the turn-on angle is set to 8° to improve the phase current balance for the fault-tolerant performance when the short-circuit fault occurs, as shown in Fig. 29(b). By the proposed fault-tolerant strategy, the torque ripple is limited in low ripple and the fault phase can still work as normal phases; therefore, the proposed fault-tolerant strategy can still apply in the 8/6 SRM. The only difference is that a phase winding can be divided into two parts for the 8/6 motor, while it is divided into three parts for the 12/8 SRM.

TABLE IV
COMPARISON OF TORQUE RIPPLE WITH AND WITHOUT FAULT-TOLERANT STRATEGY

Parameter	Without fault tolerance (PWM)	With fault tolerance (PWM)	Without fault tolerance (CCC)	With fault tolerance (CCC)
Healthy condition	0.53 N·m	0.53 N·m	0.41 N·m	0.41 N·m
Single-switch open circuit	3.1 N·m	0.56 N·m	1.96 N·m	0.46 N·m
Single-switch short circuit	8.2 N·m	0.56 N·m	10.2 N·m	0.46 N·m
All-switch fault condition	No torque generated	3.88 N·m	No torque generated	3.46 N·m

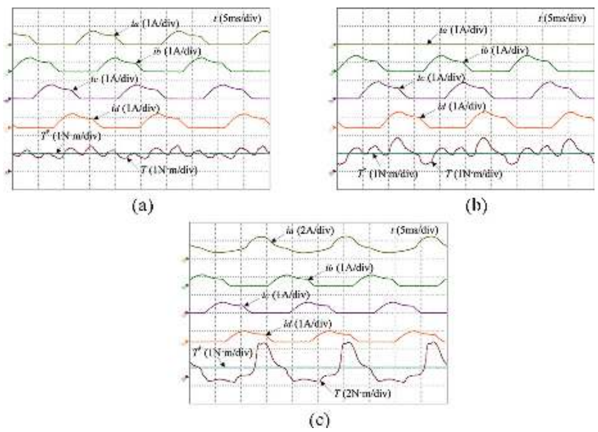

Fig. 28. Experimental results of the 8/6 SRM in voltage-PWM control mode without fault-tolerant topology under normal and fault conditions. (a) Healthy. (b) Open-circuit fault without fault-tolerant topology. (c) Short-circuit fault without fault-tolerant topology.

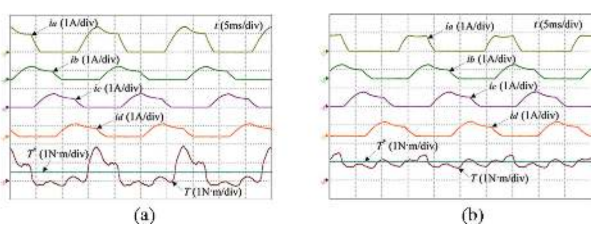

Fig. 29. Experimental results of the 8/6 SRM with fault-tolerant topology under fault conditions. (a) Fault-tolerant operation under voltage PWM control mode. (b) Turn-on angle is 8° for phase A.

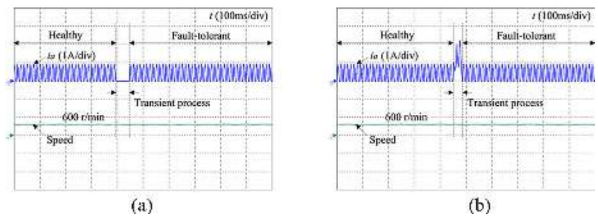

Fig. 30. Fault-diagnosis and fault-tolerant progress. (a) Open-circuit fault. (b) Short-circuit fault.

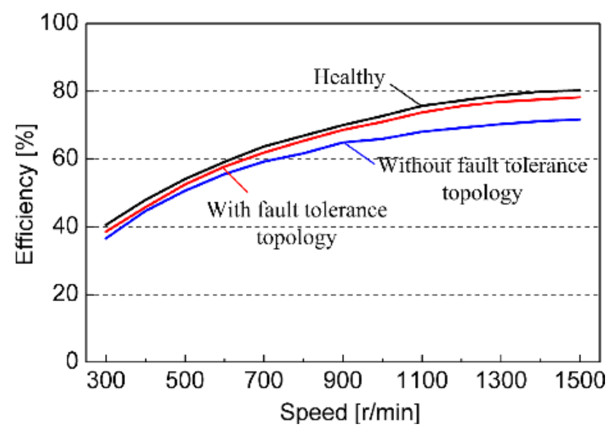

Fig. 31. SRM efficiency.

Table IV presents a comparison of torque ripples with and without the proposed fault-tolerant strategy. It can be seen that the proposed fault-tolerant strategy is effective in reducing the torque ripples. For example, under a single-switch open-circuit fault and PWM control mode, the torque ripple is 3.1 N·m without fault-tolerant strategy, which is nearly six times higher than its healthy condition. The torque ripple is reduced to 0.56 N·m when the proposed fault-tolerant strategy is implemented. When a single-switch short circuit occurs, the torque ripple is 8.2 N·m without fault-tolerant strategy, which is over 15 times of its healthy condition. It is reduced to only 0.56 N·m with the proposed fault-tolerant strategy.

Fig. 30 presents a transient progress of the system with the proposed fault-tolerant strategy. Fig. 30(a) and (b) illustrates the progress of open-circuit fault and short-circuit fault, respectively. Within 50 ms upon a fault, the proposed strategy can realize fault detection and the system can operate with the fault. Fig. 31 shows the efficiency of the SRM drive under the healthy condition, with fault-tolerant condition, and without fault-tolerant condition. For this low-power SRM prototype, the system efficiency is relatively low [38]–[41]. However, it is still very clear that the proposed fault-tolerant strategy can improve the system efficiency under fault conditions. The proposed method can effectively bypass the faulty component while still operating with healthy components in the fault phase. Without such a fault-tolerant strategy, the fault phase is lost and the system efficiency is very low.

VI. CONCLUSION

In this paper, a novel flexible topology is introduced to improve the reliability of SRM drive systems for EV/HEV applications. The main contributions of this paper are: 1) fault tolerance is achieved by developing a modular and low-cost structure, without changing traditional SRM-driving topology; 2) by the introduction of winding nodes, the traditional asymmetrical half-bridge topology is divided into three parts; by switching ON fault-tolerant part, fault diagnosis can be achieved easily; 3) for part I or part III fault, the proposed fault-tolerant topology only reduce 1/4 output; 4) when a fault occurs in one phase or faults occur in all phases, the SRM drive can still operate with the healthy parts of the fault phases, and the improved fault-tolerant operation control strategy is proposed to decrease the influence of the fault; and 5) the proposed fault-tolerant solution can be used in 12/8 and 8/6 SRMs and only needs two fault-tolerant half bridges. The developed technology can improve the reliability and cost efficiency of the SRM drive for EV/HEVs, as well as electric aircraft and ships.

REFERENCES

[1] B. K. Bose, "Global energy scenario and impact of power electronics in 21st century," *IEEE Trans. Ind. Electron.*, vol. 60, no. 7, pp. 2638–2651, Jul. 2013.

[2] S. Yantao and W. Bingsen, "Evaluation methodology and control strategies for improving reliability of HEV power electronic system," *IEEE Trans. Veh. Technol.*, vol. 63, no. 8, pp. 3661–3676, Oct. 2014.

[3] P. Pisek, B. Stumberger, T. Marcic, and P. Virtic, "Design analysis and experimental validation of a double rotor synchronous PM machine used for HEV," *IEEE Trans. Magn.*, vol. 49, no. 1, pp. 152–155, Jan. 2013.

[4] K. Kiyota, T. Kakishima, and A. Chiba, "Comparison of test result and design stage prediction of switched reluctance motor competitive with 60-kW rare-earth PM motor," *IEEE Trans. Ind. Electron.*, vol. 61, no. 10, pp. 5712–5721, Oct. 2014.

[5] H. Jinseok, L. Heekwang, and N. Kwanghee, "Charging method for the secondary battery in dual-inverter drive systems for electric vehicles," *IEEE Trans. Power Electron.*, vol. 30, no. 2, pp. 909–921, Feb. 2015.

[6] Y. Hu, X. Song, W. Cao, and B. Ji, "New SR drive with integrated charging capacity for plug-in hybrid electric vehicles (PHEVs)," *IEEE Trans. Ind. Electron.*, vol. 61, no. 10, pp. 5722–5731, Oct. 2014.

[7] I. Boldea, L. N. Tutelea, L. Parsa, and D. Dorrell, "Automotive electric propulsion systems with reduced or no permanent magnets: an overview," *IEEE Trans. Ind. Electron.*, vol. 61, no. 10, pp. 5696–5711, Oct. 2014.

[8] D. H. Lee, T. H. Pham, and J. W. Ahn, "Design and operation characteristics of four-two pole high-speed SRM for torque ripple reduction," *IEEE Trans. Ind. Electron.*, vol. 60, no. 9, pp. 3637–3643, Sep. 2013.

[9] L. Shen, J. Wu, and S. Yang, "Initial position estimation in SRM using bootstrap circuit without predefined inductance parameters," *IEEE Trans. Power Electron.*, vol. 26, no. 9, pp. 2449–2456, Sep. 2011.

[10] J. Liang, D. H. Lee, G. Xu, and J. W. Ahn, "Analysis of passive boost power converter for three-phase SR drive," *IEEE Trans. Ind. Electron.*, vol. 57, no. 9, pp. 2961–2971, Sep. 2010.

[11] M. Takeno, A. Chiba, N. Hoshi, S. Ogasawara, M. Takemoto, and M. A. Rahman, "Test results and torque improvement of the 50-kW switched reluctance motor designed for hybrid electric vehicles," *IEEE Trans. Ind. Appl.*, vol. 48, no. 4, pp. 1327–1334, Jul./Aug. 2012.

[12] C. Gan, J. Wu, S. Yang, and Y. Hu, "Phase current reconstruction of switched reluctance motors from dc-link current under double high frequency pulses injection," *IEEE Trans. Ind. Electron.*, vol. 62, no. 5, pp. 3265–3276, May 2015.

[13] B. Ji, W. Cao, P. Volker, X. Song, Y. Hu, and P. Gareth, "In-situ diagnostics and prognostics of solder fatigue in IGBT modules for electric vehicle drives," *IEEE Trans. Power Electron.*, vol. 30, no. 3, pp. 1535–1543, Mar. 2015.

[14] B. Ji, W. Cao, X. Song, Y. Hu, and V. Pickert, "Multi-objective design of IGBT power modules considering power cycling and thermal cycling," *IEEE Trans. Power Electron.*, vol. 30, no. 5, pp. 2493–2504, May 2015.

[15] H. Torkaman, E. Afjei, and P. Yadegari, "Static, dynamic, and mixed eccentricity faults diagnosis in switched reluctance motors using transient finite element method and experiments," *IEEE Trans. Magn.*, vol. 48, no. 8, pp. 2254–2264, Aug. 2012.

[16] N. S. Gameiro and A. J. Marques Cardoso, "A new method for power converter fault diagnosis in SRM drives," *IEEE Trans. Ind. Appl.*, vol. 48, no. 2, pp. 653–662, Mar./Apr. 2012.

[17] C. Hao and L. Shengli, "Fault diagnosis digital method for power transistors in power converters of switched reluctance motors," *IEEE Trans. Ind. Electron.*, vol. 60, no. 2, pp. 749–763, Feb. 2013.

[18] J. F. Marques, J. O. Estima, N. S. Gameiro, and A. M. Cardoso, "A new diagnostic technique for real-time diagnosis of power converter faults in switched reluctance motor drives," *IEEE Trans. Ind. Appl.*, vol. 50, no. 3, pp. 1854–1860, May/Jun. 2014.

[19] N. S. Gameiro and A. J. M. Cardoso, "Fault tolerant control strategy of SRM drives," in *Proc. IEEE Int. Symp. Power Electron., Electr. Drives, Autom. Motion*, Ischia, Italy, Jun. 2008, pp. 301–306.

[20] A. A. Arkadan, P. Du, M. Sidani, and M. Bouji, "Performance prediction of SRM drive systems under normal and fault operating conditions using GA-basedANN method," *IEEE Trans. Magn.*, vol. 36, no. 4, pp. 1945–1949, Jul. 2000.

[21] M. Bouji, A. A. Arkadan, and T. Ericsen, "Fuzzy inference system for the characterization of SRM drives under normal and fault conditions," *IEEE Trans. Magn.*, vol. 37, no. 5, pp. 3745–3748, Sep. 2001.

[22] A. A. Arkadan and B. W. Kielgas, "Switched reluctance motor drive systems dynamic performance prediction under internal and external fault conditions," *IEEE Trans. Energy Convers.*, vol. 9, no. 1, pp. 45–52, Mar. 1994.

[23] B. Lequesne, S. Gopalakrishnan, and A. M. Omekanda, "Winding short circuits in the switched reluctance drive," *IEEE Trans. Ind. Appl.*, vol. 41, no. 5, pp. 1178–1184, Sep./Oct. 2005.

[24] H. Torkaman and E. Afjei, "Comprehensive detection of eccentricity fault in switched reluctance machines using high-frequency pulse injection," *IEEE Trans. Power Electron.*, vol. 28, no. 3, pp. 1382–1390, Mar. 2013.

[25] M. D. Hennen, M. Niessen, C. Heyers, H. J. Brauer, and R. W. De Doncker, "Development and control of an integrated and distributed inverter for a fault tolerant five-phase switched reluctance traction drive," *IEEE Trans. Power Electron.*, vol. 27, no. 2, pp. 547–554, Feb. 2012.

[26] A. Labak and N. C. Kar, "Designing and prototyping a novel five-phase pancake-shaped axial-flux SRM for electric vehicle application through dynamic FEA incorporating flux-tube modeling," *IEEE Trans. Ind. Appl.*, vol. 49, no. 3, pp. 1276–1288, May/Jun. 2013.

[27] W. Ding, Y. Liu, and Y. Hu, "Performance evaluation of a fault-tolerant decoupled dual-channel switched reluctance motor drive under open-circuits," *IET Electr. Power Appl.*, vol. 8, no. 4, pp. 117–130, Apr. 2014.

[28] M. Ruba, I.-A. Viorel, and L. Szabo, "Modular stator switched reluctance motor for fault tolerant drive systems," *IET Electric Power Appl.*, vol. 7, no. 3, pp. 159–169, Mar. 2013.

[29] L. Szabo and M. Ruba, "Segmental stator switched reluctance machine for safety-critical applications," *IEEE Trans. Ind. Appl.*, vol. 48, no. 6, pp. 2223–2229, Nov./Dec. 2012.

[30] H. Torkaman, E. Afjei, and M. S. Toulabi, "New double-layer-per-phase isolated switched reluctance motor: concept, numerical analysis, and experimental confirmation," *IEEE Trans. Ind. Electron.*, vol. 59, no. 2, pp. 830–838, Feb. 2012.

[31] N. S. Gameiro and A. J. M. Cardoso, "Fault tolerant power converter for switched reluctance drives," in *Proc. 18th Int. Conf. Electr. Mach.*, Algarve, Portugal, Sep. 2008, pp. 1–6.

[32] M. Ruba, C. Oprea, and L. Szabó, "Comparative study on switched reluctance machine based fault-tolerant electrical drive systems," in *Proc. IEEE Int. Conf. Electric Mach. Drives*, Miami, FL, USA, May 2009, pp. 987–992.

[33] A. C. Oliveira, C. B. Jacobina, A. M. N. Lima, and F. Salvadori, "Startup and fault tolerance of the SRM drive with three-phase bridge inverter," in *Proc. IEEE Conf. Power Electron. Spec.*, Recife, Brazil, Jun. 2005, pp. 714–719.

[34] L. A. Belfore, II, and A. Arkadan, "A methodology for characterizing fault tolerant switched reluctance motors using neurogenetically derived models," *IEEE Trans. Energy Convers.*, vol. 17, no. 3, pp. 380–384, Sep. 2002.

[35] S. Mir, M. S. Islam, T. Sebastian, and I. Husain, "Fault-tolerant switched reluctance motor drive using adaptive fuzzy logic controller," *IEEE Trans. Power Electron.*, vol. 19, no. 2, pp. 289–295, Mar. 2004.

[36] W. Wang and B. Fahimi, "Fault resilient strategies for position sensorless methods of switched reluctance motors under single and multiphase fault," *IEEE J. Emerging Sel. Topics Power Electron.*, vol. 2, no. 2, pp. 190–200, Jun. 2014.

[37] Y. Hu, C. Gan, W. Cao, W. Li, and S. Finney, "Central-tapped node linked modular fault tolerance topology for SRM applications," *IEEE Trans. Power Electron.*, to be published.

[38] K. M. Rahman and S. E. Schulz, "Design of high-efficiency and high-torque-density switched reluctance motor for vehicle propulsion," *IEEE Trans. Ind. Appl.*, vol. 38, no. 6, pp. 1500–1507, Nov./Dec. 2002.

[39] D. H. Lee, J. Liang, Z. G. Lee, and J. W. Ahn, "A Simple nonlinear logical torque sharing function for low-torque ripple SR drive," *IEEE Trans. Ind. Electron.*, vol. 56, no. 8, pp. 3021–3028, Aug. 2009.

[40] J. Liang, D. H. Lee, G. Xu, and J. W. Ahn, "Analysis of passive boost power converter for three-phase SR drive," *IEEE Trans. Ind. Electron.*, vol. 57, no. 9, pp. 2961–2971, Sep. 2010.

[41] H. Y. Yang, Y. C. Lim, and H. C. Kim, "Acoustic noise/vibration reduction of a single-phase SRM using skewed stator and rotor," *IEEE Trans. Ind. Electron.*, vol. 60, no. 10, pp. 4292–4300, Oct. 2013.

Yihua Hu (M'13–SM'15) received the B.S. degree in electrical motor drives and the Ph.D. degree in power electronics and drives from the China University of Mining and Technology, Jiangsu, China, in 2003 and 2011, respectively.

Between 2011 and 2013, he was with the College of Electrical Engineering, Zhejiang University, as a Postdoctoral Fellow. Between November 2012 and February 2013, he was an Academic Visiting Scholar with the School of Electrical and Electronic Engineering, Newcastle University, Newcastle upon Tyne, U.K. He is currently a Research Associate with the Department of Electronic and Electrical Engineering, University of Strathclyde, Glasgow, U.K. His research interests include photovoltaic generation system, power electronics converters and control, and electrical motor drives.

Chun Gan (S'14) received the B.S. and M.S. degrees in power electronics and drives from the China University of Mining and Technology, Jiangsu, China, in 2009 and 2012, respectively. He is currently working toward Ph.D. degree at the College of Electrical Engineering, Zhejiang University, Hangzhou, China.

His research interests include electrical motor drives, motor design, control with emphasis on switched reluctance motor sensorless technique, and optimization of the torque ripple and efficiency of the motor system.

Wenping Cao (M'05–SM'11) received the B.Eng. degree in electrical engineering from Beijing Jiaotong University, Beijing, China, in 1991, and the Ph.D. degree in electrical machines and drives from the University of Nottingham, Nottingham, U.K., in 2004.

He is currently a Marie Curie Fellow with the Department of Electrical Engineering and Computer Science, Massachusetts Institute of Technology, Cambridge, MA, U.S.A, and a Senior Lecturer with Queen's University Belfast, Belfast, U.K. His research interests include thermal performance and fault analysis of electric machines, drives, and power electronics.

Dr. Cao received the Best Paper Award at the LDIA'13 Conference, the Innovator of the Year Award from Newcastle University, Newcastle upon Tyne, U.K., in 2013, and the Dragon's Den Competition Award from Queen's University Belfast in 2014. He serves as an Associate Editor for the IEEE TRANSACTIONS ON INDUSTRY APPLICATIONS, *IEEE Industry Applications Magazine*, *IET Power Electronics*, and nine other International journals. He is also a Member of the Institution of Engineering and Technology and a Fellow of Higher Education Academy.

Jiangfeng Zhang received the B.Sc. and Ph.D. degrees in computing mathematics and applied software from Xi'an Jiaotong University, Xi'an, China, in July 1995 and December 1999, respectively.

He is currently a Senior Lecturer at the Department of Electronic and Electrical Engineering, University of Strathclyde, Glasgow, U.K. He is also a Member of the IFAC TC6.3 (Power and Energy Systems). His research interests include optimization modeling and control of energy systems, with a focus on energy efficiency and demand side management.

Wuhua Li (M'09) received the B.Sc. and Ph.D. degrees in applied power electronics and electrical engineering from Zhejiang University, Hangzhou, China, in 2002 and 2008, respectively.

From September 2004 to March 2005, he was a Research Intern, and from January 2007 to June 2008, a Research Assistant in GE Global Research Center, Shanghai, China. From July 2008 to April 2010, he joined the College of Electrical Engineering, Zhejiang University, as a Postdoctoral Researcher. In May 2010, he became a Faculty Member at Zhejiang University as a Lecturer. In December 2010, he was promoted to an Associate Professor. From July 2010 to September 2011, he was a Postdoctoral Fellow with the Department of Electrical and Computer Engineering, Ryerson University, Toronto, ON, Canada. His research interests include high-efficiency power converters and renewable energy power conversion system. He has published more than 100 peer-reviewed technical papers and holds more than 20 issued/pending patents.

Dr. Li received the 2011 TOP TEN Excellent Young Staff Award and the 2012 Distinguished Young Scholar from Zhejiang University, the 2012 Outstanding Young Researcher Award from Zhejiang Province, the 2012 Delta Young Scholar from Delta Environmental and Educational Foundation, and the 2012 National Outstanding Young Scholar for his excellent teaching and research contributions. He received three Scientific and Technological Achievements Awards from Zhejiang Provincial Government and the State Educational Ministry of China in 2009 and 2011, respectively.

Stephen J. Finney received the M.Eng. degree from the Loughborough University of Technology, Loughborough, U.K., in 1988, and the Ph.D. degree from Heriot-Watt University, Edinburgh, U.K., in 1995.

For two years, he was with the Electricity Council Research Centre laboratories near Chester, U.K. He is currently a Professor with the University of Strathclyde, Glasgow, U.K. His research interests include HVDC, MMC, renewable generation, and electrical vehicle.